www.nature.com/aps

Acta Pharmacologica Sinica

ARTICLE

Disturbance of suprachiasmatic nucleus function improves cardiac repair after myocardial infarction by IGF2-mediated macrophage transition

Kai-li Hao[1], Qiao-cheng Zhai[2], Yue Gu[2], Yue-qiu Chen[1], Ya-ning Wang[1], Rui Liu[3], Shi-ping Yan[1], Ying Wang[4], Yu-fang Shi[3], Wei Lei[1]✉, Zhen-ya Shen[1]✉, Ying Xu[2]✉ and Shi-jun Hu[1]✉

Suprachiasmatic nucleus (SCN) in mammals functions as the master circadian pacemaker that coordinates temporal organization of physiological processes with the environmental light/dark cycles. But the causative links between SCN and cardiovascular diseases, specifically the reparative responses after myocardial infarction (MI), remain largely unknown. In this study we disrupted mouse SCN function to investigate the role of SCN in cardiac dysfunction post-MI. Bilateral ablation of the SCN (SCNx) was generated in mice by electrical lesion; myocardial infarction was induced via ligation of the mid-left anterior descending artery (LAD); cardiac function was assessed using echocardiography. We showed that SCN ablation significantly alleviated MI-induced cardiac dysfunction and cardiac fibrosis, and promoted angiogenesis. RNA sequencing revealed differentially expressed genes in the heart of SCNx mice from D0 to D3 post-MI, which were functionally associated with the inflammatory response and cytokine-cytokine receptor interaction. Notably, the expression levels of insulin-like growth factor 2 (*Igf2*) in the heart and serum IGF2 concentration were significantly elevated in SCNx mice on D3 post-MI. Stimulation of murine peritoneal macrophages in vitro with serum isolated from SCNx mice on D3 post-MI accelerated the transition of anti-inflammatory macrophages, while antibody-mediated neutralization of IGF2 receptor blocked the macrophage transition toward the anti-inflammatory phenotype in vitro as well as the corresponding cardioprotective effects observed in SCNx mice post-MI. In addition, disruption of mouse SCN function by exposure to a desynchronizing condition (constant light) caused similar protective effects accompanied by elevated IGF2 expression on D3 post-MI. Finally, mice deficient in the circadian core clock genes (*Ckm*-cre; *Bmal1*$^{f/f}$ mice or *Per1/2* double knockout) did not lead to increased serum IGF2 concentration and showed no protective roles in post-MI, suggesting that the cardioprotective effect observed in this study was mediated particularly by the SCN itself, but not by self-sustained molecular clock. Together, we demonstrate that inhibition of SCN function promotes *Igf2* expression, which leads to macrophage transition and improves cardiac repair post-MI.

Keywords: myocardial infarction; suprachiasmatic nucleus; insulin-like growth factor 2; macrophage transition; circadian core clock genes; cardioprotective effect

Acta Pharmacologica Sinica (2023) 44:1612–1624; https://doi.org/10.1038/s41401-023-01059-w

INTRODUCTION

Circadian clocks are a common feature of life on the earth, allowing physiology and behavior to be turned across the 24-daily as periodic environment. In mammals, they are coordinated by a master clock residing in the hypothalamic suprachiasmatic nucleus (SCN), which acts to receive light signals from the retina, relay the time information and synchronize the peripheral clocks in all other tissues via endocrine and autonomic signaling mechanisms [1]. The molecular clock mechanism in mammalian cells to confer circadian control of physiology is an auto-regulatory feedback of core clock genes, which consist of the trans-activating components CLOCK and BMAL1 (brain and muscle ARNT-Like 1), and the trans-inhibiting components period (PER1 and PER2) and cryptochrome (CRY1 and CRY2). While CLOCK-BMAL1 heterodimers activate the transcription of clock-controlled output genes as well as the repressor *Per* and *Cry* genes, the resulting CRY-PER heterodimers in the cytoplasm could translocate to the nucleus and further inhibit the transcriptional activation function of CLOCK-BMAL1 heterodimers. Thus, cyclical repression of CLOCK-BMAL1 activity by PER-CRY heterodimers, with additional post-transcriptional modifications, establishes ~24-h rhythms of clock-controlled genes involved in important biological processes anticipating recurring daily events [2, 3].

[1]Department of Cardiovascular Surgery of the First Affiliated Hospital & Institute for Cardiovascular Science, Collaborative Innovation Center of Hematology, State Key Laboratory of Radiation Medicine and Protection, Suzhou Medical College, Soochow University, Suzhou 215000, China; [2]Jiangsu Key Laboratory of Neuropsychiatric Diseases and Cambridge-Su Genomic Resource Center, Suzhou Medical College, Soochow University, Suzhou 215123, China; [3]The First Affiliated Hospital of Soochow University, State Key Laboratory of Radiation Medicine and Protection, Institutes for Translational Medicine, Suzhou Medical College, Soochow University, Suzhou 215123, China and [4]CAS Key Laboratory of Tissue Microenvironment and Tumor, Shanghai Institute of Nutrition and Health, Chinese Academy of Sciences, Shanghai 200031, China
Correspondence: Wei Lei (leiwei@suda.edu.cn) or Zhen-ya Shen (uuzyshen@aliyun.com) or Ying Xu (yingxu@suda.edu.cn) or Shi-jun Hu (shijunhu@suda.edu.cn)
These authors contributed equally: Kai-li Hao, Qiao-cheng Zhai, Yue Gu.

Received: 26 September 2022 Accepted: 17 January 2023
Published online: 6 February 2023

In contrast to anticipated circadian rhythms, the stress response is a rapid, demand-activated program that is essential for survival in unpredictable danger situations [4]. Stress can interfere with the molecular clock in the peripheral tissues including PERs and CRYs through the hypothalamus-pituitary-adrenal (HPA) axis to alter peripheral clock oscillation [5]. The SCN seems resistant to single exposure to acute stress, although it appears to fade away after chronic psychosocial stress [6]. The SCN neurons time the peripheral tissues through paracrine and neuronal signals to create substantial anticipation to the required moment of physiological processes, which may cause the SCN organized physiological set-points less optimally when they are exposed to unexpected acute stress. In addition to its time function, another emergent property of the SCN itself may hold suppression that may explain why ablation of the SCN improves post-stress outcomes and neurological functions. Examples include that ablation of the SCN may somehow improve memory and substantial improve body temperature homeostasis [7–9]. It is reasonable to speculate whether suppression of the SCN function or "no SCN" may be conductive upon exposure to an acute stressor.

Myocardial infarction (MI) is caused by abrupt ischemia and leads to cardiac myocyte death and compromised heart function. Cardiac repair after MI is characterized by a series of well-characterized, time-dependent events: neutrophil infiltration, which reaches a peak within 24 h, followed by monocyte recruitment to the site of injury with a peak around day 3 and an influx of pro-inflammatory monocytes that have differentiated into tissue macrophages to promote the removal of necrotic debris and tissue digestion via the release of proteolytic enzymes such as matrix metalloproteinases and cathepsin [10–12]. Subsequently, the reparative response involves a shift in the function of monocytes and macrophages toward tissue repair through increased expression of anti-inflammatory, pro-fibrotic, and angiogenic growth factors [13]. An inflammatory phase of excessive magnitude or duration is associated with adverse outcomes [14, 15]. Accordingly, our recent study found a critical role of insulin-like growth factor (IGF2) in training macrophages to exert anti-inflammatory functions [16, 17]. Thus, investigation into whether the SCN function may optimize the inflammatory response following acute MI is critical for the understanding of patho-physiological trajectories mediating risk for disease.

In the current study, we disrupted SCN function by creating lesions in the SCN or subjecting mice to desynchronizing conditions (constant light) and examined the effects on cardiac repair following acute MI. The results indicate that impairment of the SCN led to an earlier transition of activated inflammatory macrophages to repair macrophages through the production of IGF2. Additionally, treatment with IGF2 receptor (IGF2R) antibody abolished the effect of serum from mice with SCN lesions, resulting in decrease of anti-inflammatory response following MI. Importantly, administration of IGF2R antibody eliminated the beneficial effects of IGF2 on macrophages after SCN ablation and attenuated cardiac repair.

MATERIALS AND METHODS

Animal study

All experimental protocols involving animals in this study were approved by the Laboratory Animal Research Committee of Soochow University. Considering that the SCN area contains multiple modes of oestrogenic signaling, which may affect circadian regulation [18], 10- to 12-week-old male C57BL/6J mice were used in this study. Mice were housed individually in pathogen-free animal facilities and maintained under a 12-h light/dark (LD) cycle with lights on at 8: 00 (ZT0) and off at 20: 00 (ZT12) for 2 weeks before experimental manipulation, and with access to food and water *ad libitum*. The *Per1*/*Per2* double knockout mice were generated as previously reported [19]. The cardiac-specific *Bmal1*-knock out mice were generated by crossing *Ckm*-Cre (Model Animal Research Center of Nanjing University) with *Bmal1* $^{fl/fl}$ mice, offspring were genotyped by PCR for the presence of the *Bmal1* $^{fl/fl}$ alleles using gene-specific primers. All animal cages were equipped with running wheels (Clocklab, ProBeCare Scientific, Wuhan, China). For all surgeries, anesthesia was initiated by 3% isoflurane (1349003, Sigma-Aldrich, St Louis, MO, USA) and maintained by 2% isoflurane supplemented with 100% oxygen at a flow rate of 1.0 L/min during the procedure. At the end of experiments, all mice were euthanized by cervical dislocation under anesthesia with spontaneous inhalation of 3% isoflurane.

Bilateral SCN lesions were created stereotactically in C57BL/6J mice under isoflurane anesthesia. The procedure for generating the SCN lesion (SCNx) mouse model was carried out as previously described [20, 21]. Briefly, a small hole was created in the skull using a dental drill bur (0.05 mm posterior to bregma and 0.1 mm lateral from the midline). A platinum-iridium alloy electrode (0.15 mm diameter; Kedou Brain-Computer Technology, Suzhou, China) coated entirely with polyimide except for the tip (0.2 mm in length) was inserted bilaterally into the SCN (5.85 mm depth from the surface of the skull). A direct electrical current of 0.4 mA for 40 s was applied with a Ugo Basile lesion maker (model 53500, Gemonio, VA, Italy). The electrode was left in place for 1 min before withdrawal from the brain. After the SCN lesion was induced, wheel-running activities were recorded under standard LD cycles for at least 2 weeks to confirm the disturbance of circadian rhythms. For histological verification, mouse brains were fixed in 4% paraformaldehyde, sliced, and stained with the Nissl-stain. The Sham-operated mice underwent the same operation, but the electrode was inserted to a 5.4 mm depth from the skull surface, and no current was passed through the electrode.

Myocardial infarction was induced through ligation of the mid-left anterior descending artery (LAD) by an experienced microsurgeon blinded to the group as previously described [22, 23]. Briefly, the thoracic cavity was opened with micro-scissors between the third and fourth ribs to fully expose the left anterior descending coronary artery. A needle was inserted 2 mm from the lower edge of the left atrial appendage, and a suture was passed through the LAD to completely block the blood flow within the LAD. SCN sham or SCNx mice were randomized and ligated at indicated time. For IGF2R blockade in vivo, IGF2R antibody or IgG was evenly injected into the infarction heart at three points (10 μg per point), immediately following ligation of the LAD. Thereafter, the thoracic cavity was completely sutured with sutures to close the thoracic cavity. After that, ultra-high resolution small animal ultrasound imaging system Visual Sonics Vevo2100 system (Fujifilm Visualsonics, Toronto, Canada) was used to perform ultrasound examination on mice after myocardial infarction surgery [24]. All measurements were performed 3 independent operations, and the average value was taken.

Isolation and culture of macrophages

After daily injections of 3% germ-free fluid thioglycollate medium (225650, Becton, Franklin Lakes, NJ, USA) for 3 consecutive days (4 mL per day), peritoneal macrophages were harvested from mice as previously described [25]. Erythrocytes were lysed by incubation in lysis buffer (140 mmol/L NH_4Cl, 10 mmol/L Tris-HCl, pH 7.2). The peritoneal macrophages were enriched by centrifugation before seeding onto 6-well cell culture plates in RPMI-1640 containing 10% fetal bovine serum and allowed to adhere for 2 h. After removal of nonadherent cells, the remaining cells were cultured in RPMI-1640 medium until treatment with lipopolysaccharide (LPS, 100 ng/mL), interleukin-4 (IL-4, 20 ng/mL), or IGF2 (50 ng/mL) in serum-free RPMI-1640, or with 20% serum collected from Sham or SCNx mice 3 days post MI. After a 48-h treatment, macrophages were collected for further analysis.

Isolation of cardiac immune cells and flow cytometric analysis
Cardiac immune cells were collected and analyzed by flow cytometry as previously described [16, 26]. Briefly, hearts were rapidly removed from the anesthetized mice by sterile dissection, finely minced with scissors, and digested in a pre-warmed buffer containing 2% collagenase type 2, 0.25% elastase, and 0.05% DNase I (AMPD1, Sigma-Aldrich, St Louis, MO, USA). After the enzymatic reaction, the obtained cells were filtered through a 70-μm cell strainer. Immune cells were isolated by density gradient centrifugation with 37%–70% Percoll (P4937, Sigma-Aldrich, St Louis, MO, USA) according to a method described previously [27]. The cells were then stained with phycoerythrin (PE)-labeled rat anti-mouse CD45, BV605-labeled rat anti-mouse Ly-6G, allophycocyanin (APC)-cy7-labeled rat anti-mouse CD11b, PE-cy7-labeled rat anti-mouse F4/80, and APC-labeled rat anti-mouse CD206, followed by flow cytometric analysis. The information for all antibodies is listed in Supplementary Table S1.

Masson's trichrome staining and hematoxylin & eosin staining
Heart slices (sliced at 500-μm intervals from the point of ligation, with three layers assessed) were stained by Masson's trichrome staining (G1340, Solarbio, Beijing, China) and captured under stereoscopic microscope (Olympus, Tokyo, Japan). Images were then analyzed with ImageJ to determine morphometric parameters, including total left ventricle (LV) area and scar area, as described in previous studies [22]. The percentage of the total LV area occupied by the scar area was then calculated. Histologic analysis was performed using a standard hematoxylin & eosin (H&E) staining kit (G1120, Solarbio, Beijing, China) to show mononuclear cell infiltration in the infarction zone of the LV [27].

RNA preparation and sequencing (RNA-Seq)
The differentially expressed genes (DEGs) were analyzed using Cufflinks (version 2.2.1). Genes for which log2|FC|≥1 and the false discovery rate (FDR) < 0.05 were considered to be significant DEGs. The genes expression levels were normalized with Z-scores, and visualized in a heatmap generated using the R package. Functional annotation of DEGs was performed via The Database for Annotation, Visualization, and Integrated Discovery (DAVID) (https://david.ncifcrf.gov/). Gene Ontology (GO) and Kyoto Encyclopedia of Genes and Genomes (KEGG) pathway enrichment analyses were conducted. Functional Gene Set Enrichment Analysis (fGSEA) was performed via the GSEA R/Bioconductor package, and the log2|FC|value for each gene calculated by Cufflinks (version 2.2.1) was used as the ranking metric input.

Quantitative real-time polymerase chain reaction (qRT-PCR)
Samples for total RNA isolation were stored in RNA stabilization solution, and RNA was extracted using Invitrogen™ TRIzol™ reagent (15596026, Waltham, MA, USA). Thereafter, the single-strand complementary DNA was reverse-transcribed using the TaKaRa PrimeScript™ RT Reagent Kit (RR037Q, Clontech, San Francisco, CA, USA). Real-time PCR detection was performed using the StepOnePlus™ Real-Time PCR System (Applied Biosystems, Carlsbad, CA, USA). Data were analyzed using $2^{-\Delta\Delta CT}$ method and normalized to *18S* rRNA. All primer sequences are listed in Supplementary Table S2.

Western blot analysis
For preparing total protein samples from cells exposed to specific treatments, cells were harvested using radioimmunoprecipitation (RIPA) lysis buffer supplemented with a protease inhibitor cocktail. The protein samples were subjected to denaturing 10% sodium dodecyl sulfate-polyacrylamide gel electrophoresis (SDS-PAGE) and transferred onto polyvinylidene difluoride (PVDF) membranes. Proteins of interest within the membranes were bound with corresponding antibodies and visualized using the Phototope-HRP Western blot detection system (Cell Signaling Technology, Danfoss, MA, USA). The information for all antibodies is listed in Supplementary Table S1.

Immunofluorescence staining
Tissue sections and cultured cells were fixed in 4% paraformaldehyde in phosphate-buffered saline (PBS) solution for 15 min and then permeabilized with 0.1% Triton X-100 in PBS (only for intracellular markers) for 15 min before being blocked with 5% normal donkey serum for 1 h at room temperature and then incubated with primary antibodies at 4 °C overnight. After incubation with fluorescent-labeled secondary antibodies for 1 h at room temperature, cells or sections were counterstained with DAPI and observed on an inverted fluorescent microscope (Zeiss, Oberkochen, Germany).

Detection of serum IGF2
The concentrations of insulin-like growth factor 2 (IGF2) level was determined using ELISA kit (JL10182, Jianglai Bio, Shanghai, China). Briefly, the mice serum samples were incubated at 37 °C with antibodies coated flat bottom plates. Then the plates were washed with PBS with 10% fetal bovine serum. The horseradish peroxidase (HRP)-conjugated secondary antibody was added to the plates for 15 min and absorbance was read at 405 nm using the plate reader (Biotek, Santa Clara, CA, USA).

Statistical analysis
Statistical comparisons between two groups were conducted using Student's *t*-test. Comparisons among multiple groups were made with one-way analysis of variance (ANOVA) or two-way repeated-measures ANOVA with the Bonferroni post-hoc test. Statistical significance was denoted by a P value of less than 0.05. All data are presented as mean ± standard error of the mean (SEM). All experimental assays were performed at least three times.

RESULTS

Ablation of the SCN attenuates cardiac impairment after MI in mice
To assess the function of the SCN in the response to an acute stressor, we performed bilateral ablation of the SCN (SCNx), which was shown previously to abolish circadian synchronization from the SCN [9], and used Chi-square periodogram analysis of locomotor rhythms to screen arrhythmic mice (Fig. 1a). At the end of the experiment, histological analyses of the brains in the Sham-operated and SCNx mice confirmed the formation of SCN lesions (Fig. 1b).

Since the time-of-day of ischemia onset was reported to affect the myocardial infarct size and subsequent cardiac function [28], we first investigated the effects of SCN on the outcome of MI occurred at different zeitgeber times (ZT). All animal experiments were performed in a double-blind manner. Sham-operated and SCNx mice were subjected to experimental MI during resting (ZT5) or active (ZT13) phase (Fig. 1c), and cardiac function in these mice was assessed by echocardiography on days 0, 3, 5, 7, 10, 14, and 28 post-MI. No significant cardiac physiological difference was detected between SCNx and Sham-operated mice when assessed via echocardiography on day 0 (Fig. 1d–g). Consistent with previous studies [28], Sham-operated mice subjected to LAD ligation at ZT13 indicated more severe myocardial injury when compared to mice with MI at ZT5 from day 3 post-MI. However, SCNx mice undergoing MI did not show such time-of-day-dependent change in cardiac injury (Fig. 1d–g). When compared with Sham-operated mice, SCNx mice abided MI surgery at ZT5 or ZT13 showed less cardiac impairment from day 5 post-MI, as evidenced by increases in left ventricular ejection fraction (LVEF) and left ventricular fractional shortening (LVFS), and a decrease in the left ventricular internal dimension systole (LVIDs) (Fig. 1d–g).

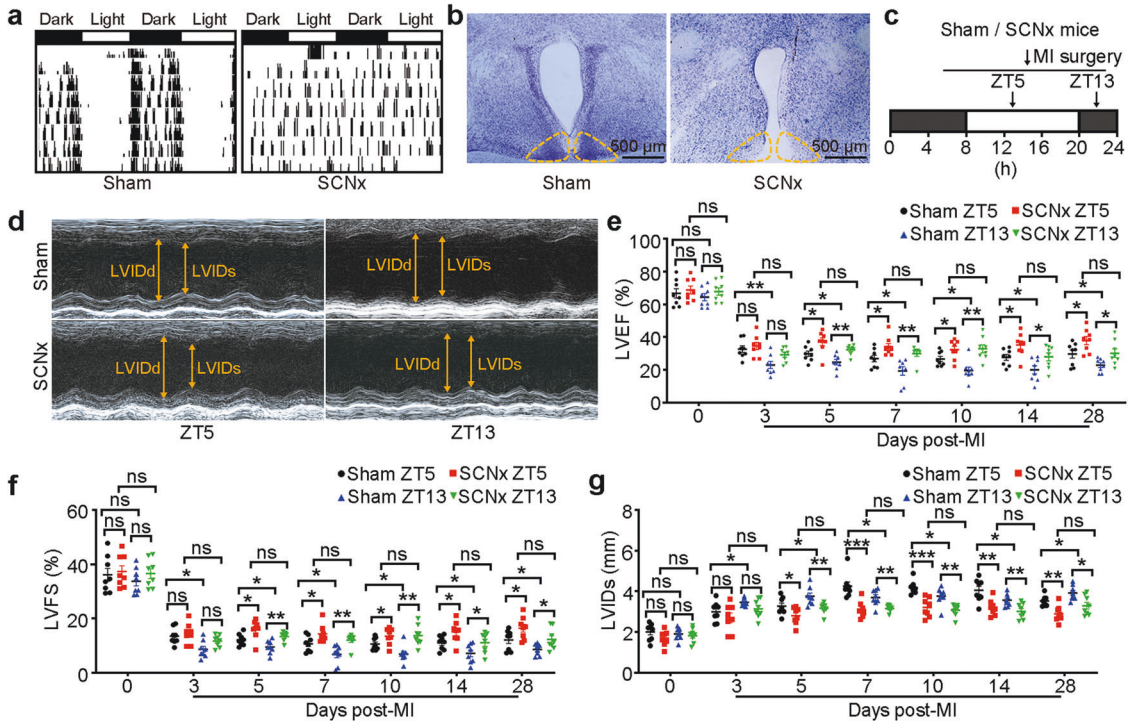

Fig. 1 SCN ablation in mice attenuated MI-induced cardiac injury during ZT5 and ZT13. a Representative double-plotted locomotor actograms after ablation of the SCN. Periods of darkness and light are indicated by black and white bars, respectively. **b** The lesioned areas in the SCN of mice were confirmed by Nissl staining (Scale bar: 500 μm). **c** Schematic diagram of permanent LAD occlusion for myocardial infarction (MI) surgery was performed at ZT5 or ZT13. (ZT, zeitgeber time). **d** Representative M-mode echocardiographic images obtained from SCNx mice and Sham-operated mice on day 28 post-MI at ZT5 and ZT13 (heart rate: 450–500 bpm). **e** LVEF assessed via echocardiography at the indicated time points after MI ($n = 8$ per group). **f** LVFS at the indicated time points after MI ($n = 8$ per group). **g** LVIDs at the indicated time points after MI ($n = 8$ per group). Data are presented as mean ± SEM; two-way repeated-measures ANOVA; $^{*}P < 0.05$, $^{**}P < 0.01$, $^{***}P < 0.001$, ns: not significant.

These improvements in cardiac function were consistent with reduction in cardiac fibrosis in SCNx mice compared with Sham-operated mice in both ZT5 and ZT13 surgical groups (Fig. 2a). In accordance with the histologic findings, the expression levels of fibrosis-associated genes including *α-SMA* and *Col1a1* and their proteins were obviously reduced in the infarcted heart of SCNx mice (Fig. 2b–d). Additionally, ablation of the SCN increased the number of $CD31^{+}$ endothelial cells (ECs) in the border zone of the SCNx mice determined by immunofluorescence (Fig. 2e). Expression of the EC-associated biomarkers *Cd31* and *Vwf* was significantly higher in the hearts of SCNx mice than in those of Sham-operated MI mice, indicating that ablation of the SCN promoted vascular regeneration in response to MI (Fig. 2f). Altogether, SCN lesions showed equivalently protective function after MI surgery both at ZT5 and ZT13.

To exclude confounding effects of stress induced by the surgical procedure, we also created lesions in a non-SCN region of the lateral hypothalamic nucleus that regulates appetite and hunger (non-SCNx mice) and assessed the effects on cardiac function post-MI (Supplementary Fig. S1). As expected, no significant differences in the basic pathophysiology of MI were observed between the Sham-operated and non-SCNx mice, implying that the protective effect on cardiac function post-MI was derived specifically from the disturbance of SCN function.

To further verify that the observed protection of cardiac function is derived from the SCN, we exposed mice to constant light for 2 weeks (LL mice), which has been shown to desynchronize the SCN neurons and cause arrhythmicity [29], and then applied the MI model (Supplementary Fig. S2a). As expected, the LL mice showed attenuation of LV remodeling and LV function reservation from day 3 post-MI, as indicated by increases in LVEF and LVFS and decreases in LVIDs and cardiac fibrosis (Supplementary Fig. S2b–f), indicating that suppression of SCN function again has a beneficial effect on MI-induced cardiac function recovery. To distinguish the roles of the SCN itself and molecular clock, we examined this protective role in *Per1*/*Per2* double knockout mice, which are deficient in behavioral and molecular circadian rhythms [19]. In response to MI, no protective effect on post-MI cardiac function was observed in *Per1*/*Per2* double knockout mice, in contrast to that seen in SCNx mice and LL mice, and indeed, even more deterioration of pathophysiologic function (Supplementary Fig. S3a–e) and cardiac fibrosis (Supplementary Fig. S3f) was observed, implying the inhibitory effect on MI-induced cardiac impairment is specifically dependent on the disruption of SCN.

Collectively, these data indicate that SCN-mediated ventricular remodeling post-MI is most likely function of the SCN itself rather than a function of the self-sustained molecular clock.

Ablation of the SCN advances the time-dependent inflammatory process following MI

Notably, the protective effect of SCN lesions on cardiac pathophysiological function was detectable on day 5 post-MI, which corresponds the timing of the transition from inflammatory response to reparative response [30]. We hypothesized that suppression of SCN function can affect the early inflammatory response before new homeostasis is established. We tested this hypothesis by high-throughput transcriptome profiling of the left ventricle tissues of Sham-operated and SCNx mice on days 0, 3, and 5 post-MI ($n = 3$, each group) at ZT5, as disruption of the SCN abolishes the time difference between ZT5 and ZT13. A total of 160, 139, and 101 DEGs (SCNx/Sham, adjusted *P*-value <0.05 and $|\log2\text{Ratio}| \geq 1$) were identified in mouse heart at days 0, 3, and 5

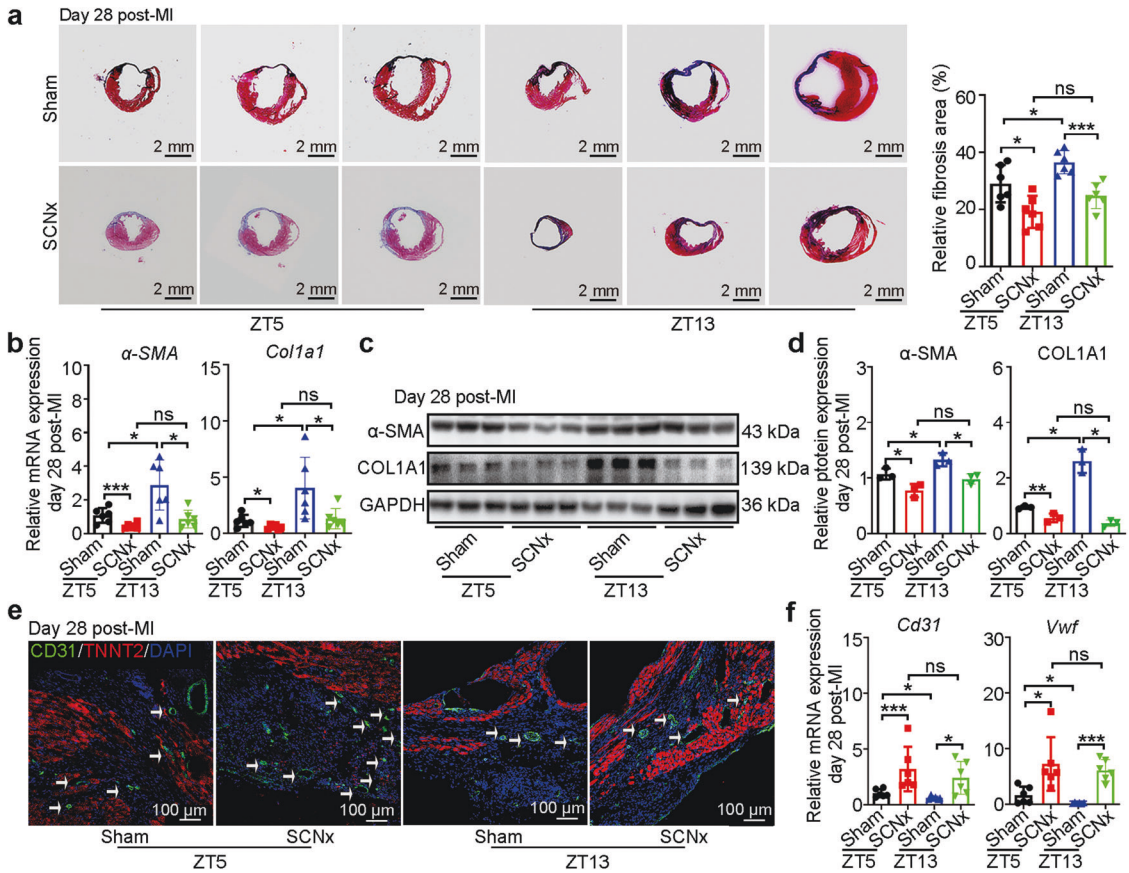

Fig. 2 SCN ablation in mice ameliorated MI-induced cardiac fibrosis and promoted angiogenesis. a Representative images of Masson's trichrome-stained MI hearts, and quantification of fibrosis (% area) showing a significant decrease in fibrosis areas in MI hearts from SCNx mice (Scale bars: 2 mm, $n = 6$ per group). **b** The qRT-PCR analysis of *α-SMA* and *Col1a1* expression as indicators of myocardial fibrosis ($n = 6$ per group). **c** Western blot analysis and relative densitometric quantification (**d**) of α-SMA and COL1A1 protein expression in MI hearts ($n = 3$ per group). **e** Representative images of immunofluorescence staining for CD31 and TNNT2, and quantification of angiogenesis in the border zone of heart post-MI (Scale bar: 100 μm). **f** The qRT-PCR analysis of *Cd31* and *Vwf* expression in the infarction zone of MI hearts as indicators of the heart's angiogenic ability ($n = 6$ per group). Data are presented as mean ± SEM; one-way ANOVA; $^{*}P < 0.05$, $^{***}P < 0.001$, ns not significant.

post-MI, respectively. Furthermore, the DEGs statistics showed that only rare percentage of genes are normally expressed in the heart with circadian rhythmicity, indicating that circadian genes are not the main regulators in this process (Supplementary Table S3).

GO and KEGG enrichment analysis indicates that DEGs at day 3 are mainly involved in inflammation-related pathways (Fig. 3a–e), and DEGs at both days 0 and 5 are enriched in ECM-related pathways (Supplementary Fig. S4a–e and Supplementary Fig. S6a–e). However, the expression patterns of these ECM-relative genes between Sham-operated and SCNx mice were reversed at days 0 (down-regulation) and 5 (up-regulation) post-MI (Supplementary Fig. S4e and Supplementary Fig. S6e). In addition, many genes for ECM components were activated specifically in the infarcted myocardium of SCNx mice in the early post-MI phase (days 0 to 3) (Supplementary Fig. S5).

Moreover, analysis of GSEA for KEGG on days 0, 3, and 5 post-MI found enrichment of IL-17 signaling pathway, indicating SCN lesions was closely related to inflammatory responses (Fig. 3d, Supplementary Fig. S4d, and Supplementary Fig. S6d). As what mentioned before, we analyzed day 3 samples and distinguished 96 up-regulated genes and 43 down-regulated genes between the SCNx and Sham samples (Fig. 3a, b). The GO analysis of these DEGs showed biological process of inflammatory responses and chemokines regulation, which indicated that the inflammatory response mainly played the significant role in SCN lesioned mice after MI compared with Sham group (Fig. 3c). GSEA for KEGG revealed that SCN lesions resulted in defective chemokine pathway and the expression levels of CCL chemokines (pro-inflammatory genes *Ccl6* and *Ccl9*, anti-inflammatory genes *Ccl2*、*Ccl4* and *Ccl7*) were significantly increased [31–35], which predicted that chemokines were both positively or negatively regulated inflammatory responses on day 3 post-MI (Fig. 3d, e).

Remarkably, insulin like growth factor (IGF) cytokine gene expression was reversed between day 0 and day 3 samples (Fig. 3f and Supplementary Fig. S4f). In the day 0 samples, wound healing genes related *Igfbp2*, *Igfbp3* and *Igfbp5* were all down-regulated after SCN disruption [36–38], which was consistent with ECM gene expression (Supplementary Fig. S4d–f). Besides, pro-inflammatory gene *Igfals* was significantly up-regulated after SCN lesions [39], however, the expression of anti-inflammatory gene *Igf2* was comparable [16], indicating SCN lesions may lead to a pro-inflammatory response. In the day 3 samples, IGF-related cytokines showed significant increase in the SCN-lesioned group, notably, *Igfals* expression was down-regulated with suppressed pro-inflammatory responses (Fig. 3f). Among them, the expression levels of *Igf2* were increased on days 3 post-MI in SCNx mice (Fig. 3f). Our recent study found that IGF2 enables macrophages to acquire anti-inflammatory abilities [16]. Therefore, in addition to the aforementioned reduction of pro-inflammatory and acceleration of cytokines function, IGF2 may exert its effects by influencing the anti-inflammatory capabilities of macrophages. Altogether, these data suggest that disruption of the SCN affects the basic molecular signatures and specific biological response to MI through regulation of cytokine and immune system in the early response phase.

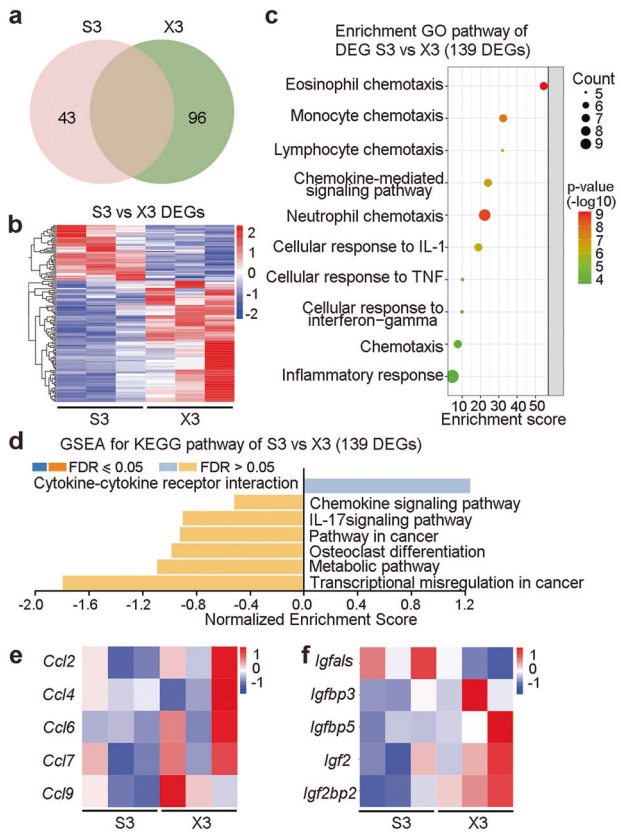

Fig. 3 SCN ablation led to the changes on cardiac transcriptome on day 3 post-MI. a Summary of the DEGs on day 3 post-MI between left ventricle tissues from the Sham-operated and SCNx mice. **b** Heatmap of DEGs between Sham mice on day 3 post-MI and SCNx on day 3 post-MI. **c** Analysis of significant GO terms in genes that were dysregulated by at least 2-fold between Sham on day 3 post-MI and SCNx on day 3 post-MI. **d** GSEA for KEGG pathway in Sham and SCNx mice left ventricle tissue on day 3 post-MI. **e** Heatmap of gene of CCL chemokines between Sham on day 3 post-MI and SCNx on day 3 post-MI. **f** Heatmap of IGF-related genes between Sham and SCNx on day 3 post-MI. S3, Sham on day 3 post-MI; X3, SCNx on day 3 post-MI.

In addition, the expression of IGF-related cytokines showed no change on day 5, suggesting that IGF2 is likely to play a regulatory role on day 3 (Supplementary Fig. S6f).

Ablation of the SCN facilities macrophage transition

To validate above changes in molecular signatures, the infarcted tissues were examined by H&E staining and showed obviously greater inflammatory cell infiltration in the SCNx mice compared with the Sham-operated mice in independent MI cohorts (Fig. 4a). Therewith we detected and found that the gene expression of anti-inflammatory cytokines *Il-10*, *Cd206* and *Arg1* were significantly increased in the infarcted LV of SCNx mice on day 3 post-MI compared with those in Sham-operated mice based on qRT-PCR analysis in independent MI cohorts (Fig. 4b). However, the expression levels of pro-inflammatory cytokines *Tnf-α, Il-1β*, and *iNOS* did not differ significantly between the two groups (Fig. 4c). From Western blot analysis, the trends in protein expression levels were in agreement with those for RNA expression levels (Fig. 4d, e). These results suggest that disruption of the SCN causes an earlier and stronger anti-inflammatory response.

The inflammatory response gives way to an anti-inflammatory response mediated in large part by an influx of pro-inflammatory monocytes that differentiate into tissue macrophages [12], as characterized by the release of anti-inflammatory factors. Our transcriptome analysis above is considered to reflect a hybrid function in SCNx mice was due to changes in macrophage subpopulations, we used iNOS as a marker for pro-inflammatory macrophages and CD206 as a marker for anti-inflammatory macrophages with counterstaining with the F4/80 molecule, a unique marker of murine macrophages [40, 41] (i.e., $iNOS^+F4/80^+$ indicated pro-inflammatory and $CD206^+F4/80^+$ indicated anti-inflammatory cells). The distribution of $iNOS^+F4/80^+$ cells showed no difference between SCNx and Sham-operated mice (Fig. 4f). In contrast, the ratio of $CD206^+F4/80^+$ cells was higher in the infarcted LV of SCNx mice than in the Sham-operated mice (Fig. 4g). These changes are consistent with the increased CD206 expression in SCNx mice on day 3 post-MI (Fig. 4b, d and e), supporting that ablation of the SCN facilitates an environment for anti-inflammatory response following MI.

Considering macrophage heterogeneity, we conducted flow cytometric analyses to further assess macrophage diversity in the infarcted site (Fig. 4h and Supplementary Fig. S7). On day 3 post-MI, the proportion of macrophages sorted as $CD45^+$ $CD11b^+$ $Ly\text{-}6G^-$ $F4/80^+$ ($leukocyte^+/monocyte^+/neutrophils^-/macrophage^+$) was obviously increased in the infarcted LV of SCNx mice compared to the Sham-operated MI mice (Fig. 4h and Supplementary Fig. S7). Furthermore, the number of macrophages expressing CD206 was much higher in SCNx mice than in Sham-operated mice (Fig. 4h and Supplementary Fig. S7), suggesting that macrophage accumulation in the infarcted region was mainly derived from the infiltration of monocytes. Altogether, these data suggest that ablation of the SCN facilitates the transition of some inflammatory macrophages toward an anti-inflammatory phenotype in early repair and ventricular remodeling.

IGF2 promotes macrophage transition in SCNx mice

Based on our findings that macrophages derived from circulating monocytes exhibited a decreased pro-inflammatory response and increased reparative response following MI in the SCNx mice, we reasoned that serum from SCNx mice might facilitate macrophage reprogramming. To test this ability of SCNx serum, we stimulated murine peritoneal macrophages with serum isolated from Sham and SCNx mice on day 3 post-MI, using separate LPS and IL-4 treatments as positive controls for induction of pro-inflammatory and anti-inflammatory macrophages, respectively. We analyzed the effects of serum collected from SCNx mice post-MI on gene expression levels in macrophages. *Il-10*, *Cd206*, and *Arg1* were significantly upregulated in macrophages treated with serum from SCNx mice collected post-MI or with IL-4, but not in those treated with serum from Sham-operated mice or with LPS (Fig. 5a). In contrast to this upregulation of anti-inflammatory molecules, the pro-inflammatory molecules *Tnf-α*, *Il-1β* and *iNOS* were not upregulated in macrophages treated with IL-4 or serum from SCNx mice post-MI, but were increased by LPS treatment (Fig. 5b). Western blot analysis produced consistent results, with increased CD206 and AGR1 production by macrophages exposed to serum derived from SCNx mice post-MI or IL-4 but not by those treated with serum from Sham-operated mice post-MI or LPS. As a control, LPS treatment did induce accumulation of IL-1β and iNOS (Fig. 5c, d). These results suggest that serum from SCNx mice subjected to MI likely have a major effect on the macrophage transition.

As in the transcript analysis described above, the expression of *Igf2* in SCNx mice 3 days post-MI was comparatively higher than that in Sham-operated mice 3 days post-MI (Fig. 3f). We reasoned that the increased expression of IGF2 might promote macrophage transition toward anti-inflammatory capacity. First, we validated the expression level of *Igf2* based on qRT-PCR analysis in independent MI cohorts. Consistent with the RNA-Seq analysis, *Igf2* expression is significantly increased in the infarcted LV of SCNx mice on day 3 post-MI compared with those in Sham-operated mice (Fig. 5e). Then we measured the IGF2 content in

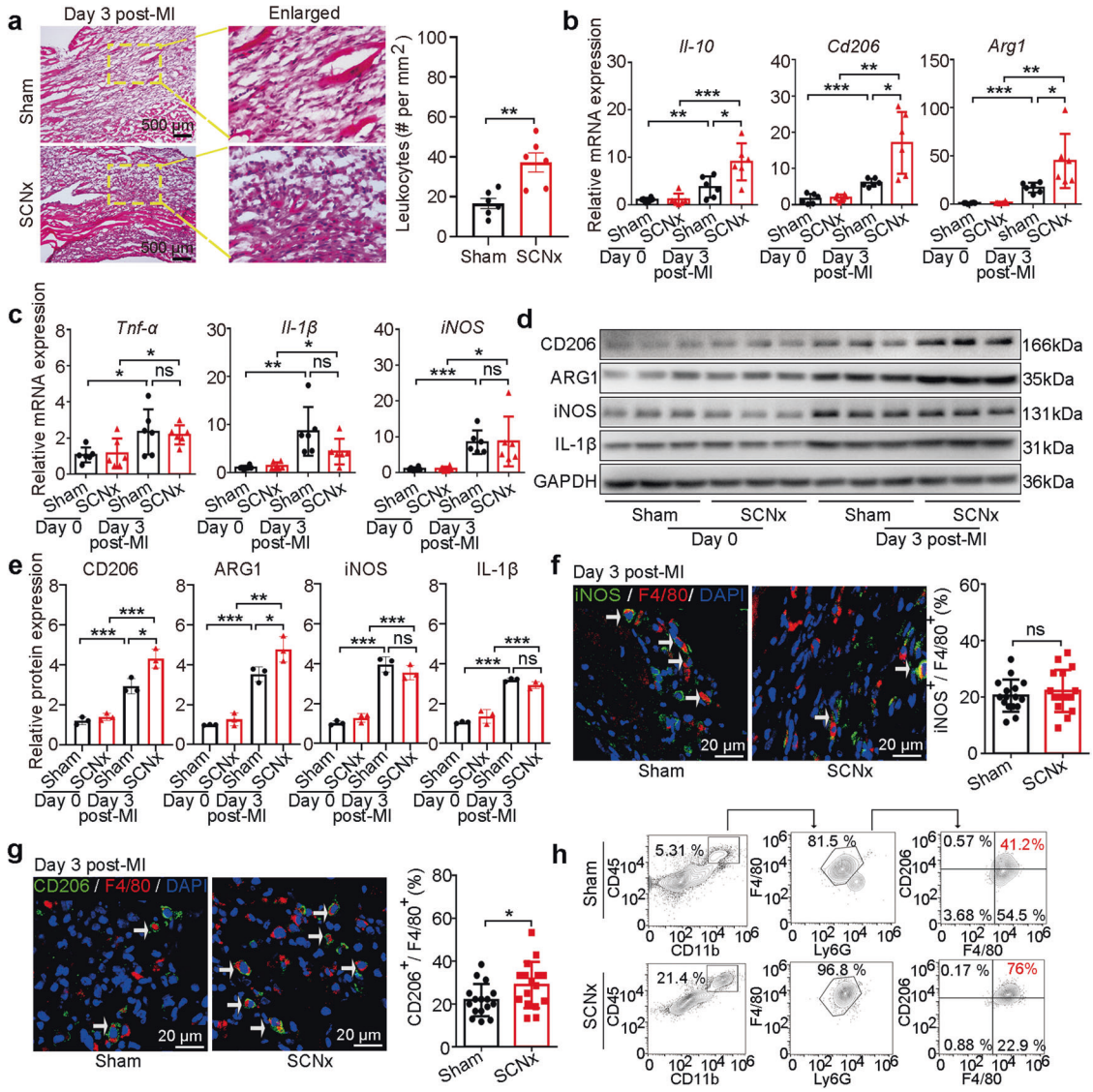

Fig. 4 SCN ablation modulated anti-inflammatory macrophage switch in the mouse heart post-MI. a H&E staining and quantitative analysis of leukocytes (dark blue-purple monocytes) in the infarcted zone in the Sham-operated and SCNx mice on day 3 post-MI (Scale bars: 500 μm). **b** Gene expression levels of anti-inflammatory markers *Il-10*, *Cd206*, and *Arg1* in the LV of Sham-operated and SCNx mice on days 0 and 3 post-MI ($n = 6$ per group). **c** Gene expression levels of pro-inflammatory markers *Tnf-α*, *Il-1β*, and *iNOS* in the LV of Sham-operated and SCNx mice on days 0 and 3 post-MI ($n = 6$ per group). **d** Western blot analysis of CD206, ARG1, IL-1β, and iNOS protein levels in infarcted hearts on day days 0 and 3 post-MI ($n = 3$ per group). **e** Relative densitometric quantification of CD206, ARG1, IL-1β, and iNOS protein levels in infarcted hearts on day 3 post-MI ($n = 3$ per group). **f** Representative immunofluorescence staining images and quantitative analysis showing $iNOS^+$ and $F4/80^+$ macrophages in the infarcted hearts of Sham-operated and SCNx mice on day 3 post-MI (Scale bars: 20 μm, $n = 16$ per group). **g** Representative immunofluorescence staining images and quantitative analysis showing $CD206^+$ and $F4/80^+$ macrophages in the infarcted heart of Sham-operated and SCNx mice on day 3 post-MI (Scale bars: 20 μm, $n = 16$ per group). **h** Flow cytometric analyses of the $CD45^+$ $CD11b^+$ $Ly\text{-}6G^-$ $F4/80^+$ $CD206^+$ macrophages in the infarcted hearts of Sham-operated and SCNx mice ($n = 4$ per group). Data are presented as mean ± SEM; Student's *t*-test or one-way ANOVA; $^*P < 0.05$, $^{**}P < 0.01$, $^{***}P < 0.001$, ns not significant.

serum collected from the two groups of mice on day 3 post-MI and found that the IGF2 concentration was significantly higher in the serum of SCNx mice than in the serum of Sham-operated serum (Fig. 5f and Supplementary Fig. S8a). In addition to this, IGF2 content in the serum of SCNx mice and Sham-operated mice on day 0 before MI was comparable (Supplementary Fig. S8b), which indicates the increase of IGF2 inhibits myocardial injury in the early stage of myocardial infarction. Then, we confirmed that the IGF2 did increase the expression of *Il-10*, *Cd206*, and *Arg1*, but not of inflammatory factors such as *Tnf-α*, *Il-1β*, and *iNOS*, in macrophages treated with IGF2 (Supplementary Fig. S9a–d), suggesting that ablation of SCN mediates elevation of IGF2 in heart and serum which promotes the macrophage switch to an anti-inflammatory phenotype.

Finally, to identify whether the macrophage switch induced by serum derived from SCNx mice post-MI is caused by elevated IGF2 expression, we added IGF2 receptor (IGF2R) antibody to the serum collected from SCNx mice post-MI, as described in our previous studies [16, 17]. Transcript and immunoblot analyses revealed that treatment with 1 μg/mL IGF2R antibody sufficiently blocked the macrophage switch induced by serum from SCNx mice post-MI [17, 42] (Fig. 5g–i). These results indicate that IGF2 expression following MI in SCNx mice plays an important role on the macrophage transition toward the anti-inflammatory phenotype.

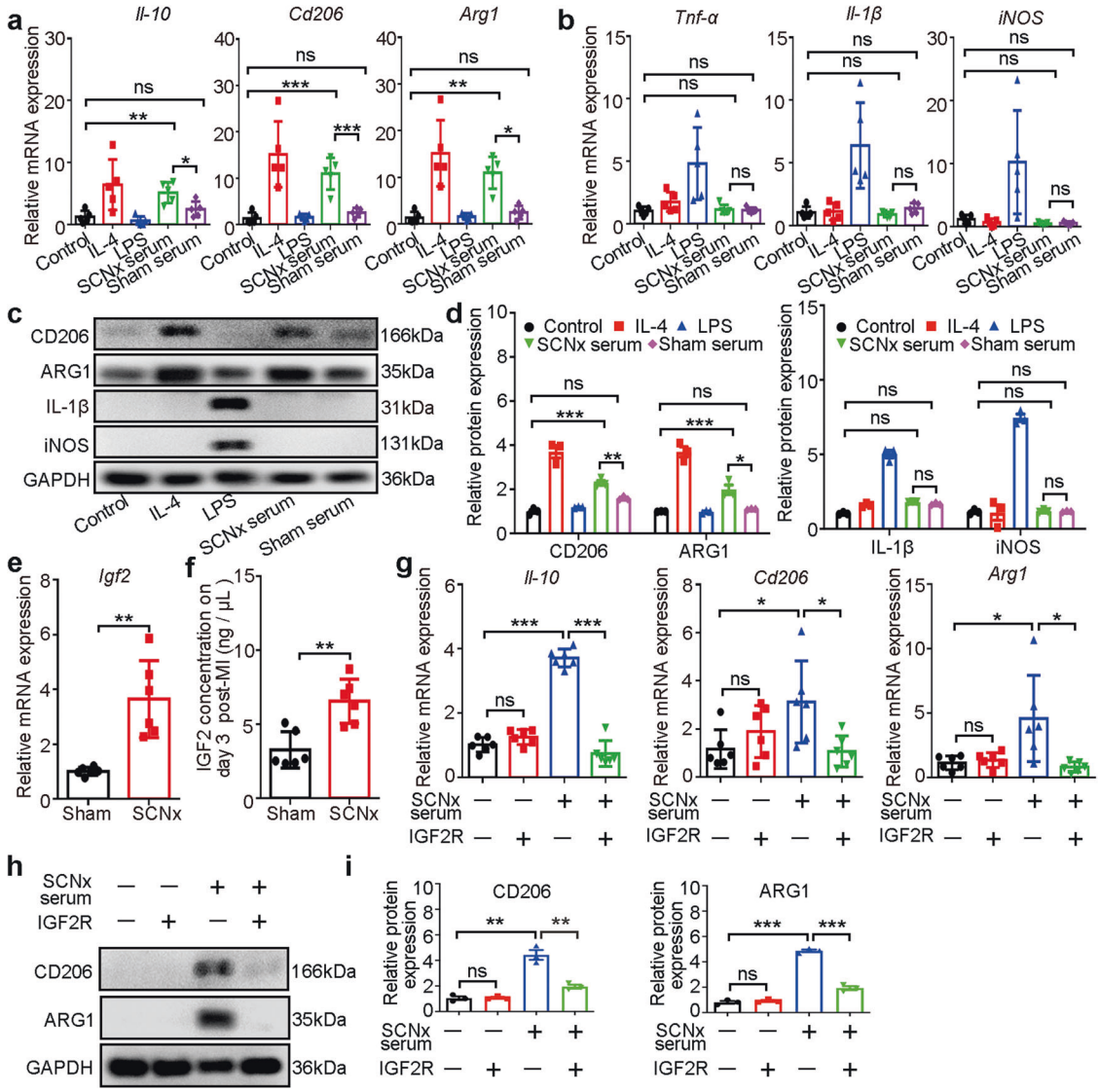

Fig. 5 IGF2 promoted macrophage reprogramming in SCNx mice. a The qRT-PCR analysis of anti-inflammatory macrophage markers *Il-10*, *Cd206*, and *Arg1* ($n = 6$ per group). The macrophages were treated for 48 h with IL-4 (20 ng/mL), LPS (100 ng/mL), and serum collected from Sham-operated or SCNx mice on day 3 post-MI. **b** The qRT-PCR analysis of M1 macrophage markers *Tnf-α*, *Il-1β*, and *iNOS* ($n = 6$ per group). **c** Western blot analysis of CD206, ARG1, IL-1β, and iNOS protein levels in the isolated peritoneal macrophages treated with IL-4 (20 ng/mL), LPS (100 ng/mL), and serum collected from Sham-operated or SCNx mice on day 3 post-MI ($n = 3$ per group). **d** Relative densitometric quantification of CD206, ARG1, IL-1β, and iNOS protein levels in the isolated peritoneal macrophages after the specified treatments ($n = 3$ per group). **e** The qRT-PCR analysis of *Igf2* expression in the LV of Sham-operated and SCNx mice on day 3 post-MI ($n = 6$ per group). **f** IGF2 protein concentration in the serum of Sham-operated and SCNx mice on day 3 post-MI (excitation wavelength=450 nm; $n = 6$ per group). **g** The qRT-PCR analysis of specific markers in macrophages after the specified treatments ($n = 6$ per group). **h** Relative densitometric quantification of CD206 and ARG1 protein levels in IGF2R antibody-untreated or IGF2R antibody-treated macrophages after exposure to SCNx mouse serum ($n = 3$ per group). **i** Relative densitometric quantification of CD206 and ARG1 protein levels in the isolated peritoneal macrophages after the specified treatments ($n = 3$ per group). Data are presented as mean ± SEM; *Student's t*-test or one-way ANOVA; $^{*}P < 0.05$, $^{**}P < 0.01$, $^{***}P < 0.001$, ns not significant.

Treatment with IGF2R antibody abolishes the protective effect of SCN ablation against MI-induced cardiac injury

To verify whether the protective role of SCN ablation after MI is mediated by IGF2, we administered IGF2R antibody or IgG into the infarct area in the hearts of Sham-operated and SCNx mice immediately after MI. The cardiac dimensions and function were monitored by echocardiography on days 0, 3, 5, 7, 10, 14, and 28 after MI (Fig. 6a). The analyses revealed that IGF2R antibody administration caused the decreases in the LVEF and LVFS, as well as an increase in LVIDs both in Sham and SCNx mice (Fig. 6b–e) from day 7 post-MI. It is worth noting that Sham mice showed poor cardiac function compared with the SCNx mice from day 3 post-MI due to the inhibitory effect of IGF2R antibody (Fig. 6b–e), indicating importance of IGF2 involved in regulating cardiac function after the SCN ablation mice with MI. Consistent with these results, we also observed an enlargement of cardiac fibrosis in the injured mouse heart after IGF2R antibody injection (Fig. 7a). The gene and protein expression levels of fibrosis-related factors including *α-SMA* and *Col1a1* examined by qRT-PCR and Western blot, respectively, were significantly increased in the IGF2R antibody injection group (Figs. 7b–d). In addition, compared with the IgG injection group, we observed a decreased amount of $CD31^{+}$ ECs in the border zone of the IGF2R antibody injection group (Fig. 7e). Furthermore, the *Cd31* and *Vwf* mRNA expression

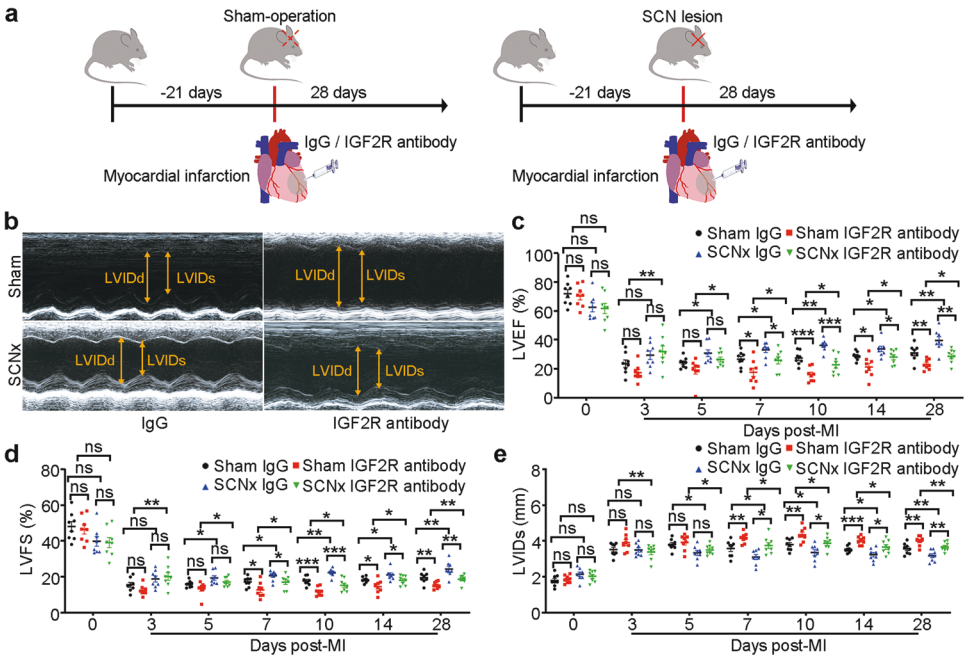

Fig. 6 IGF2R antibody treatment abolished the protective effect of SCN ablation against MI-induced cardiac injury. a Schematic diagram of IGF2R antibody treatment in the MI heart, showing antibody injection (10 μg) into the infarcted heart at three points. **b** Representative M-mode echocardiographic images from mice after IgG injection or IGF2R antibody injection on day 28 post-MI (heart rate: 450–500 bpm). **c** LVEF as assessed via echocardiography at the indicated time points post-MI ($n = 8$ per group). **d** LVFS at the indicated time points post-MI ($n = 8$ per group). **e** LVIDs at the indicated time points post-MI ($n = 8$ per group). Data are presented as mean ± SEM; two-way repeated-measures ANOVA; $^{*}P < 0.05$, $^{**}P < 0.01$, $^{***}P < 0.001$, ns not significant.

levels were also reduced, indicating that IGF2R antibody injection led to the inhibition of angiogenesis in the SCNx mice (Fig. 7f).

Notably, we also observed that the proportion of $CD206^{+}$ and $F4/80^{+}$ macrophages was obviously reduced in IGF2R antibody-injected SCNx mice on day 3 post-MI, and the proportion of $CD206^{+}$ and $F4/80^{+}$ anti-inflammatory macrophages in Sham mice with IGF2R injection is the lowest (Fig. 7g), which is most likely due to the neutralization of elevated IGF2 produced in Sham and SCNx mice, which would otherwise have induced the macrophage transition toward the anti-inflammatory phenotype. To unequivocally demonstrate that elevated IGF2 on day 3 post-MI plays a key role in the protective effect of SCN dysfunction, we analyzed the expression of IGF2 in mice exposed to constant light (LL condition) and found that there is a similar elevation of IGF2 on day 3 post-MI (Fig. S10), in consistent with the protective effect by LL (Supplementary Fig. S2).

Next, we tested whether disruption of other circadian clock genes also induced IGF2 expression, and we found no changes in the level of IGF2 on day 3 post-MI in *Per1/2* double knockout mice (Supplementary Fig. S11), consistent with the observation that disruption of *Per1/2* expression did not attenuate cardiac dysfunction post-MI. In parallel, we generated tissue-specific conditional *Bmal1* knockout mice (*Ckm*-cre; $Bmal1^{f/f}$) under control of the muscle creatine kinase (Ckm) promoter, which is expressed in skeletal and cardiac muscle. The results of immunoassay analysis showed no significant difference in IGF2 expression on day 3 post-MI between control and *Ckm*-cre; $Bmal1^{f/f}$ mice (Supplementary Fig. S12). Altogether, these data further suggest that disruption of SCN function, but not the self-sustained molecular clock, is a much more potent inducer of IGF2 production in the early response to MI.

DISCUSSION

The circadian clock and stress systems are both fundamental for survival, and their functions are known to be highly interconnected. The circadian clock regulates the activation of the stress response system before the active phase begins and then its deactivation at the end of the active phase [43]. Accumulating evidence suggests that exposure to repeated stress will lead to dysfunction of the circadian clock, resulting in a pathological response [44]. However, in present study, we found that while Sham-operated mice showed the time-of-day dependence of MI tolerance in heart, disturbance of SCN function with the creation of lesions in the SCN or desynchronization of the SCN by constant light exposure actually reduced cardiac dysfunction following acute MI, suggesting that the functional SCN may negatively affect cardiac repair mechanisms after MI providing causative links between the SCN and MI tolerance. Our data further demonstrate that increased IGF2 expression induced by SCN ablation accelerated the transition of activated inflammatory macrophages to reparative anti-inflammatory macrophages, suggesting a likely mechanism for the protective effect of SCN ablation against MI-induced cardiac injury (Fig. 8).

Previous research has shown that disruption of circadian rhythm and circadian rhythm genes affects the heart rate, myocardial contractility, and energy metabolism, which altogether leads to ischemia [45–47]. Unlike our approach that disrupts SCN in advance, recent studies showed that the disruption of environment light-dark cycle post-MI could worsen ventricular remodeling [48, 49], which might due to the sensitivity of MI mouse on the drastic circadian rhythm change. Furthermore, altered expression of the circadian genes is associated with MI [50], *Per2* shows cardioprotective function via mitochondrial translocation [49, 51], meanwhile, *Bmal1* knockout or cardiomyocyte-specific deletion of *Bmal1* in mice, which is known to abolish all circadian rhythms, causes abnormal cardiac metabolism and dilated cardiomyopathy [52, 53]. In the present study, deletion of *Per1/2*, which results in arrhythmic behavior in mice, also resulted in worsened cardiac function after MI. These worsen ventricular remodeling after MI was not observed in the SCN lesioned mice. Furthermore, the expression of IGF2 in *Ckm*-cre; $Bmal1^{f/f}$ mice or *Per1/2* knockout mice was not induced after MI, suggesting that the profective role of the SCN lesions is

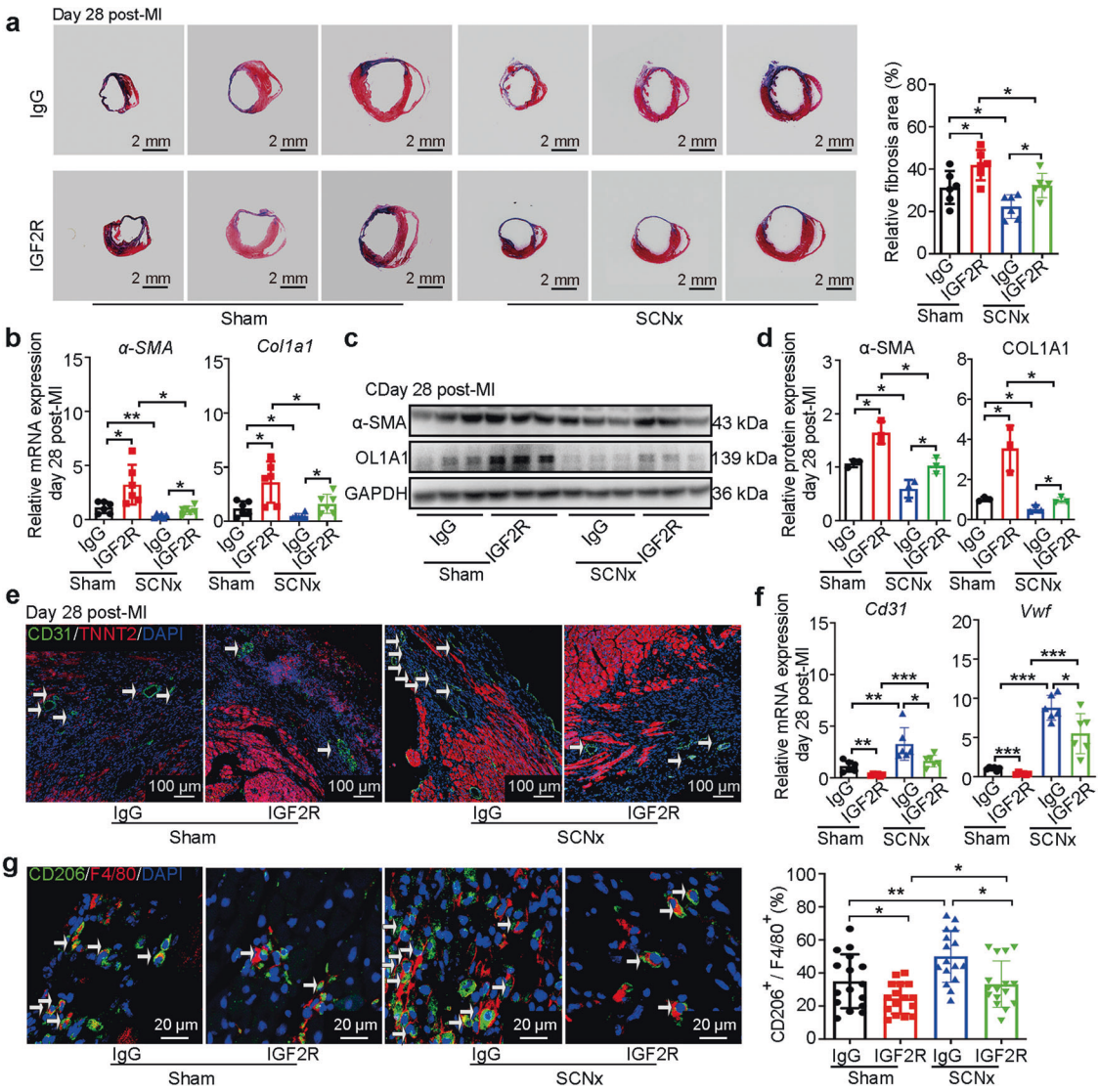

Fig. 7 IGF2R antibody treatment disturbed anti-fibrotic and anti-inflammatory effect of SCN ablation. a Representative images of Masson's trichrome-stained MI hearts, and quantification of fibrosis (% area) showing a significant increase in the fibrosis areas in IGF2R antibody-injected MI hearts (Scale bars: 2 mm, $n = 6$ per group). **b** The qRT-PCR analysis of *α-SMA*and *Col1a1* expression as indicators of myocardial fibrosis ($n = 6$ per group). Western blot analysis (**c**) and relative densitometric quantification of α-SMA and COL1A1 (**d**) protein levels in MI hearts ($n = 3$ per group). **e** Representative images of immunofluorescence staining for CD31 and TNNT2, and quantification of angiogenesis in the border zone of the heart after MI (Scale bar: 100 μm). **f** The qRT-PCR analysis of *Cd31* and *Vwf* in the infarction zone of MI hearts as indicators of the heart's angiogenic ability ($n = 6$ per group). **g** Representative immunofluorescence staining images and quantitative analysis showing $CD206^+$ and $F4/80^+$ macrophages in the hearts of Sham-operated and SCNx mice on day 3 post-MI (Scale bars: 20 μm, $n = 16$ per group). Data are presented as mean ± SEM; two-way repeated-measures ANOVA; $^*P < 0.05$, $^{**}P < 0.01$, $^{***}P < 0.001$.

different from the role of the molecular clock. Despite evidence for the potential adverse effects of chronic disruption of the circadian clock [48, 49, 54, 55], very little is known about the role of the SCN in the response to acute stress including MI. We proposed that the SCN may hold a general suppression function on some physiological processes in addition to its circadian function.

Here we addressed the hypothesis that a functional SCN limits the ability to quickly respond to acute MI. Some examples in nature support the concept of disturbance of SCN function to adapt to the environment variation, such as the loss of circadian behavior in reindeer and the Svalbard ptarmigan during the period of 24 h of daylight in the arctic summer season [56, 57]. In addition, our previous study found that SCN ablation rescued mice from the lethality of time-restricted feeding otherwise induced by the loss of body temperature homeostasis under an ambient temperature 21 °C [9]. These observations suggested that the stress created by an extreme environment may exert some control over SCN processing adaptation and the SCN inhibits body temperature homeostasis during extreme environment. Interestingly, in the present study, we again found that ablation of the SCN had a protective effect in response to acute stress generated by MI. Another previous study showed that intense light (10000 lux; 14: 10 h light: dark phase) also had a cardioprotective function based on reduced infarct sizes after myocardial ischemia, which was mediated by amplification of a PER2-dependent metabolic pathway [51]. An obvious difference between this previous study and the present study is the use of a PER2-enhancing strategy to disrupt the circadian clock system in the previous study versus desynchronization of the SCN by light intervention (200 lux; constant light) and ablation of the SCN in the present study, although the consequences were somewhat similar. Thus, the potential role of phototherapy as a cardioprotective treatment will

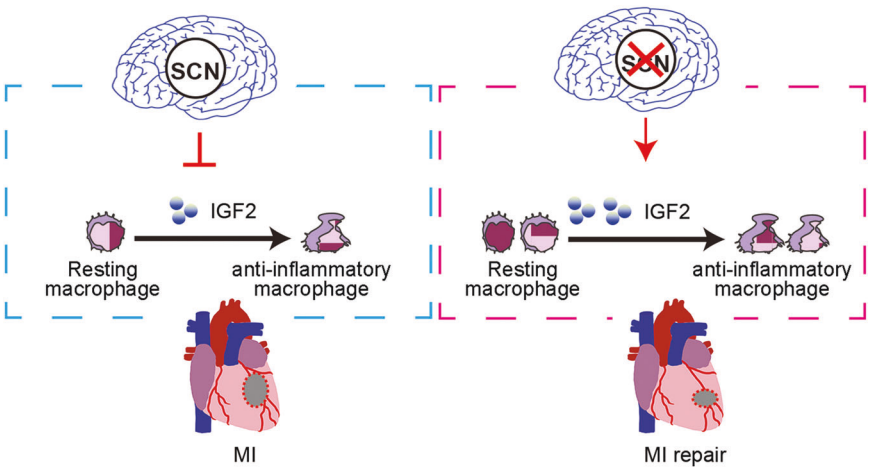

Fig. 8 Disturbance of suprachiasmatic nucleus function preserves cardiac function by IGF2-mediated macrophage transition. Schematic cartoon illustrating the protective mechanism of SCN ablation against MI in mice: the increased expression of IGF2 in SCNx mice promotes localized resting macrophage transition into anti-inflammatory macrophages in the heart and eventually preserves cardiac function by promoting angiogenesis and inhibiting fibrosis in the infarcted heart.

be interesting to explore, but the possible involvement of SCN-related arrythmia in the cardioprotective mechanism should be considered carefully.

Previous research showed that bilateral lesions of the SCN result in an increased inflammatory response to LPS, demonstrating that interaction between the SCN and the immune system modulates the intensity of the inflammatory response [58]. In the present study, we unexpectedly found that the lesioned SCN-induced elevated serum expression of IGF2. IGF2 shares similarities with the B chain of insulin, but is not suppressed by insulin antibody [59]. IGF2 is largely produced by the choroid plexus epithelium in the developing brain [60]. In general, the dynamics of IGF2 concentration in the serum seems to correlate with *Igf2* mRNA expression in peripheral tissue [61]. In addition to its functions in tumor growth, progression, and metabolism [62], IGF2 is a critical mitogen in cardiac development [63]. Our recent study showed that IGF2 plays important roles in regulating the immune response under pathophysiological conditions [16], suggesting IGF2 plays an important regulatory role in both physiological and pathological stages of the heart. The results of the present study indicate that increased IGF2 in serum or/and *Igf2* mRNA in post-MI heart induced by SCN ablation facilitates the transition of pro-inflammatory macrophages to anti-inflammatory macrophages during the response to MI-induced injury, which consequently improves cardiac function. These findings suggest that the effect of IGF2 on macrophages is key in the early stage following MI.

Our study indicated a protective effect of SCN disruption on MI-induced myocardial injury, which is probably mediated by systemic effects of acute stress response or paracrine and neuronal signal response in vivo. Although, the intervention of SCN in clinical application is still unclear so far, however, light seems to stimulate biochemical reactions and activate one or more molecules or cells in the body, such as immune cells, inflammatory mediators, or bone marrow-derived stem cells [17], light may act as a way to intervene in SCN. In addition, developing non-invasive SCN interference methods and investigating the function of SCN interference in ischemia-reperfusion models could promote the clinical translation of this strategy.

One restriction in this study is how to translate the finding to clincal non-invasive SCN intervene application. Our study indicated a protective effect of SCN disruption on MI-induced myocardial injury, which is probably mediated by systemic effects of acute stress response or paracrine and neuronal signal response in vivo. However, the invasive method for SCN disruption is not suitable clinical application. Alternately, our study showed that light may act as a way to intervene SCN function. In addition, developing other non-invasive SCN interference methods and investigating the function of SCN interference in ischemia-reperfusion models could promote the clinical translation of this strategy. Additionally, the study is insufficient to linearly illustrate how SCN regulate IGF2 release in myocardial infarction, although we clearly prove that SCN disturbance improves cardiac repair by IGF2-induced macrophage transformation. Following studies are needed to explore the mechanism and would provide the basis to formulate MI intervention strategy.

CONCLUSIONS

Taken together, our results show that the SCN negatively regulates stress response induced by MI and IGF2 is a key link between the SCN and reparative process following MI. IGF2 may serve as a new target for early intervention in myocardial infarction. However, the underlying mechanisms for the relationship between SCN and IGF2 activation remain to be determined. Our results demonstrate an unexpected effect of the SCN in the hypothalamus on the remodeling of myocardial infarction and the inhibitory function of SCN in increasing protective effect after MI. The latter indicates that the coupling between the SCN and peripheral tissues, while beneficial under normal conditions, may have detrimental physiological effects under stress response. Therefore, additional research to demonstrate whether the SCN negatively regulates the response to acute stress is warranted.

ACKNOWLEDGEMENTS

This study was supported by the National Key R&D Program of China (2022YFA1104300, 2018YFA0801100, 2021YFA1101902), the National Natural Science Foundation of China (82241202, 31630091, 82170364, 81970223), the Priority Academic Program Development of the Jiangsu Higher Education Institutes (PAPD) and National Center for International Research (2017B01012), the Natural Science Foundation of Jiangsu Province (BK20201409), Jiangsu Province's Key Discipline/Laboratory of Medicine (XK201118) and Introduction Project of Clinical Medicine Expert Team for Suzhou (SZYJTD201704), Lingang Laboratory & National Key Laboratory of Human Factors Engineering Joint Grant (LG-TKN-202203-01).

AUTHOR CONTRIBUTIONS

KLH performed the heart-related experiment. QCZ performed bilateral SCN lesions in mice and conducted other clock mutant mice models. YG worked on RNA-Seq data analysis. YQC and RL performed flow cytometric analysis. YNW and SPY performed immunofluorescence staining. YFS, YW, WL, ZYS, YX, and SJH conceived and

designed the experiments. KLH, WL, YX, and SJH wrote the manuscript. All authors read, edited, and approved the manuscript.

ADDITIONAL INFORMATION

Supplementary information The online version contains supplementary material available at https://doi.org/10.1038/s41401-023-01059-w.

Competing interests: The authors declare no competing interests.

REFERENCES

1. Hastings MH, Maywood ES, Brancaccio M. Generation of circadian rhythms in the suprachiasmatic nucleus. Nat Rev Neurosci. 2018;19:453–69.
2. Rabinovich-Nikitin I, Lieberman B, Martino TA, Kirshenbaum LA. Circadian-regulated cell death in cardiovascular diseases. Circulation. 2019;139:965–80.
3. Gentry NW, Ashbrook LH, Fu YH, Ptáček LJ. Human circadian variations. J Clin Invest. 2021;131:e148282.
4. Ellis BJ, Del Giudice M. Developmental adaptation to stress: an evolutionary perspective. Annu Rev Psychol. 2019;70:111–39.
5. Oster H. The interplay between stress, circadian clocks, and energy metabolism. J Endocrinol. 2020;247:R13–R25.
6. Helfrich-Forster C. Interactions between psychosocial stress and the circadian endogenous clock. Psych J. 2017;6:277–89.
7. Ruby NF. Suppression of circadian timing and its impact on the hippocampus. Front Neurosci. 2021;15:642376.
8. Fernandez F, Lu D, Ha P, Costacurta P, Chavez R, Heller HC, et al. Circadian rhythm. Dysrhythmia in the suprachiasmatic nucleus inhibits memory processing. Science. 2014;346:854–7.
9. Zhang Z, Zhai Q, Gu Y, Zhang T, Huang Z, Liu Z, et al. Impaired function of the suprachiasmatic nucleus rescues the loss of body temperature homeostasis caused by time-restricted feeding. Sci Bull. 2020;65:1268–80.
10. Chazaud B. Macrophages: supportive cells for tissue repair and regeneration. Immunobiology. 2014;219:172–8.
11. Chen B, Huang S, Su Y, Wu YJ, Hanna A, Brickshawana A, et al. Macrophage smad3 protects the infarcted heart, stimulating phagocytosis and regulating inflammation. Circ Res. 2019;125:55–70.
12. Nahrendorf M, Pittet MJ, Swirski FK. Monocytes: protagonists of infarct inflammation and repair after myocardial infarction. Circulation. 2010;121:2437–45.
13. Hilgendorf I, Gerhardt LM, Tan TC, Winter C, Holderried TA, Chousterman BG, et al. Ly-6Chigh monocytes depend on Nr4a1 to balance both inflammatory and reparative phases in the infarcted myocardium. Circ Res. 2014;114:1611–22.
14. Frangogiannis NG. Regulation of the inflammatory response in cardiac repair. Circ Res. 2012;110:159–73.
15. Prabhu SD, Frangogiannis NG. The biological basis for cardiac repair after myocardial infarction: from inflammation to fibrosis. Circ Res. 2016;119:91–112.
16. Du L, Lin L, Li Q, Liu K, Huang Y, Wang X, et al. IGF-2 preprograms maturing macrophages to acquire oxidative phosphorylation-dependent anti-inflammatory properties. Cell Metab. 2019;29:1363–75. e8
17. Wang X, Lin L, Lan B, Wang Y, Du L, Chen X, et al. IGF2R-initiated proton rechanneling dictates an anti-inflammatory property in macrophages. Sci Adv. 2020;6:eabb7389.
18. Vida B, Hrabovszky E, Kalamatianos T, Coen CW, Liposits Z, Kalló I. Oestrogen receptor alpha and beta immunoreactive cells in the suprachiasmatic nucleus of mice: distribution, sex differences and regulation by gonadal hormones. J Neuroendocrinol. 2008;20:1270–7.
19. Zheng B, Albrecht U, Kaasik K, Sage M, Lu W, Vaishnav S, et al. Nonredundant roles of the mPer1 and mPer2 genes in the mammalian circadian clock. Cell. 2001;105:683–94.
20. Saleh MA, Winget CM. Effect of suprachiasmatic lesions on diurnal heart rate rhythm in the rat. Physiol Behav. 1977;19:561–4.
21. Mohawk JA, Baer ML, Menaker M. The methamphetamine-sensitive circadian oscillator does not employ canonical clock genes. Proc Natl Acad Sci USA. 2009; 106:3519–24.
22. Han X, Zhao ZA, Yan S, Lei W, Wu H, Lu XA, et al. CXADR-like membrane protein protects against heart injury by preventing excessive pyroptosis after myocardial infarction. J Cell Mol Med. 2020;24:13775–88.
23. Fang X, Miao S, Yu Y, Ding F, Han X, Wu H, et al. MIR148A family regulates cardiomyocyte differentiation of human embryonic stem cells by inhibiting the DLL1-mediated NOTCH signaling pathway. J Mol Cell Cardiol. 2019;134:1–12.
24. Yu Y, Qin N, Lu XA, Li J, Han X, Ni X, et al. Human embryonic stem cell-derived cardiomyocyte therapy in mouse permanent ischemia and ischemia-reperfusion models. Stem Cell Res Ther. 2019;10:167.
25. Shi C, Sakuma M, Mooroka T, Liscoe A, Gao H, Croce KJ, et al. Down-regulation of the forkhead transcription factor Foxp1 is required for monocyte differentiation and macrophage function. Blood. 2008;112:4699–711.
26. Yan X, Anzai A, Katsumata Y, Matsuhashi T, Ito K, Endo J, et al. Temporal dynamics of cardiac immune cell accumulation following acute myocardial infarction. J Mol Cell Cardiol. 2013;62:24–35.
27. Wang J, Liu M, Wu Q, Li Q, Gao L, Jiang Y, et al. Human embryonic stem cell-derived cardiovascular progenitors repair infarcted hearts through modulation of macrophages via activation of signal transducer and activator of transcription 6. Antioxid Redox Signal. 2019;31:369–86.
28. Schloss MJ, Horckmans M, Nitz K, Duchene J, Drechsler M, Bidzhekov K, et al. The time-of-day of myocardial infarction onset affects healing through oscillations in cardiac neutrophil recruitment. EMBO Mol Med. 2016;8:937–48.
29. Ohta H, Yamazaki S, McMahon DG. Constant light desynchronizes mammalian clock neurons. Nat Neurosci. 2005;8:267–9.
30. Peet C, Ivetic A, Bromage DI, Shah AM. Cardiac monocytes and macrophages after myocardial infarction. Cardiovasc Res. 2020;116:1101–12.
31. Farid AS, El Shemy MA, Nafie E, Hegazy AM, Abdelhiee EY. Anti-inflammatory, anti-oxidant and hepatoprotective effects of lactoferrin in rats. Drug Chem Toxicol. 2021;44:286–93.
32. Liu Y, Cai Y, Liu L, Wu Y, Xiong X. Crucial biological functions of CCL7 in cancer. PeerJ. 2018;6:e4928.
33. Shen Z, Kuang S, Zhang M, Huang X, Chen J, Guan M, et al. Inhibition of CCL2 by bindarit alleviates diabetes-associated periodontitis by suppressing inflammatory monocyte infiltration and altering macrophage properties. Cell Mol Immunol. 2021;18:2224–35.
34. Qian BZ, Li J, Zhang H, Kitamura T, Zhang J, Campion LR, et al. CCL2 recruits inflammatory monocytes to facilitate breast-tumour metastasis. Nature. 2011;475: 222–5.
35. Kanno M, Suzuki S, Fujiwara T, Yokoyama A, Sakamoto A, Takahashi H, et al. Functional expression of CCL6 by rat microglia: a possible role of CCL6 in cell-cell communication. J Neuroimmunol. 2005;167:72–80.
36. Martín AI, Priego T, Moreno-Ruperez Á, González-Hedström D, Granado M, López-Calderón A. IGF-1 and IGFBP-3 in inflammatory cachexia. Int J Mol Sci. 2021;22:9469.
37. Faramia J, Hao Z, Mumphrey MB, Townsend RL, Miard S, Carreau AM, et al. IGFBP-2 partly mediates the early metabolic improvements caused by bariatric surgery. Cell Rep Med. 2021;2:100248.
38. Xiang A, Chu G, Zhu Y, Ma G, Yang G, Sun S. IGFBP5 suppresses oleate-induced intramyocellular lipids deposition and enhances insulin signaling. J Cell Physiol. 2019;234:15288–98.
39. Flannery BM, Amuzie CJ, Pestka JJ. Evaluation of insulin-like growth factor acid-labile subunit as a potential biomarker of effect for deoxynivalenol-induced proinflammatory cytokine expression. Toxicology. 2013;304:192–8.
40. Jablonski KA, Amici SA, Webb LM, Ruiz-Rosado Jde D, Popovich PG, Partida-Sanchez S, et al. Novel markers to delineate murine M1 and M2 macrophages. PLoS One. 2015;10:e0145342.
41. Mosser DM, Edwards JP. Exploring the full spectrum of macrophage activation. Nat Rev Immunol. 2008;8:958–69.
42. Sandovici I, Georgopoulou A, Pérez-García V, Hufnagel A, López-Tello J, Lam BYH, et al. The imprinted Igf2-Igf2r axis is critical for matching placental microvasculature expansion to fetal growth. Dev Cell. 2022;57:63–79. e8
43. Agorastos A, Nicolaides NC, Bozikas VP, Chrousos GP, Pervanidou P. Multilevel interactions of stress and circadian system: implications for traumatic stress. Front Psychiatry. 2019;10:1003.
44. Nicolaides NC, Charmandari E, Kino T, Chrousos GP. Stress-related and circadian secretion and target tissue actions of glucocorticoids: impact on health. Front Endocrinol. 2017;8:70.
45. McAlpine CS, Swirski FK. Circadian influence on metabolism and inflammation in atherosclerosis. Circ Res. 2016;119:131–41.
46. Rabinovich-Nikitin I, Rasouli M, Reitz CJ, Posen I, Margulets V, Dhingra R, et al. Mitochondrial autophagy and cell survival is regulated by the circadian clock gene in cardiac myocytes during ischemic stress. Autophagy 2021;17:3794–812.
47. Knutsson A, Hallquist J, Reuterwall C, Theorell T, Akerstedt T. Shiftwork and myocardial infarction: a case-control study. Occup Environ Med. 1999;56:46–50.
48. Alibhai FJ, Tsimakouridze EV, Chinnappareddy N, Wright DC, Billia F, O'Sullivan ML, et al. Short-term disruption of diurnal rhythms after murine myocardial infarction adversely affects long-term myocardial structure and function. Circ Res. 2014;114:1713–22.
49. Wang Y, Jiang W, Chen H, Zhou H, Liu Z, Liu Z, et al. Sympathetic nervous system mediates cardiac remodeling after myocardial infarction in a circadian disruption model. Front Cardiovasc Med. 2021;8:668387.
50. Škrlec I, Milic J, Heffer M, Peterlin B, Wagner J. Genetic variations in circadian rhythm genes and susceptibility for myocardial infarction. Genet Mol Biol. 2018; 41:403–9.

51. Oyama Y, Bartman CM, Bonney S, Lee JS, Walker LA, Han J, et al. Intense light-mediated circadian cardioprotection via transcriptional reprogramming of the endothelium. Cell Rep. 2019;28:1471–84. e11
52. Lefta M, Campbell KS, Feng HZ, Jin JP, Esser KA. Development of dilated cardiomyopathy in Bmal1-deficient mice. Am J Physiol Heart Circ Physiol. 2012;303:H475–85.
53. Liang Q, Xu H, Liu M, Qian L, Yan J, Yang G, et al. Postnatal deletion of Bmal1 in cardiomyocyte promotes pressure overload induced cardiac remodeling in mice. J Am Heart Assoc. 2022;11:e025021.
54. Song S, Tien CL, Cui H, Basil P, Zhu N, Gong Y, et al. Myocardial Rev-erb-mediated diurnal metabolic rhythm and obesity paradox. Circulation. 2022;145:448–64.
55. Durgan DJ, Pulinilkunnil T, Villegas-Montoya C, Garvey ME, Frangogiannis NG, Michael LH, et al. Short communication: ischemia/reperfusion tolerance is time-of-day-dependent: mediation by the cardiomyocyte circadian clock. Circ Res. 2010;106:546–50.
56. van Oort BE, Tyler NJ, Gerkema MP, Folkow L, Blix AS, Stokkan KA. Circadian organization in reindeer. Nature. 2005;438:1095–6.
57. Stokkan KA, Mortensen A, Blix AS. Food intake, feeding rhythm, and body mass regulation in Svalbard rock ptarmigan. Am J Physiol. 1986;251:R264–7.
58. Guerrero-Vargas NN, Salgado-Delgado R, Basualdo Mdel C, García J, Guzmán-Ruiz M, Carrero JC, et al. Reciprocal interaction between the suprachiasmatic nucleus and the immune system tunes down the inflammatory response to lipopolysaccharide. J Neuroimmunol. 2014;273:22–30.
59. Rinderknecht E, Humbel RE. The amino acid sequence of human insulin-like growth factor I and its structural homology with proinsulin. J Biol Chem. 1978;253:2769–76.
60. Fernandez AM, Torres-Alemán I. The many faces of insulin-like peptide signalling in the brain. Nat Rev Neurosci. 2012;13:225–39.
61. Beletskiy A, Chesnokova E, Bal N. Insulin-like growth factor 2 as a possible neuroprotective agent and memory enhancer-its comparative expression, processing and signaling in mammalian CNS. Int J Mol Sci. 2021;22:1849.
62. Clayton PE, Banerjee I, Murray PG, Renehan AG. Growth hormone, the insulin-like growth factor axis, insulin and cancer risk. Nat Rev Endocrinol. 2011;7:11–24.
63. Shen H, Gan P, Wang K, Darehzereshki A, Wang K, Kumar SR, et al. Mononuclear diploid cardiomyocytes support neonatal mouse heart regeneration in response to paracrine IGF2 signaling. Elife. 2020;9:e53071.